Large-scale oscillatory calcium waves in the immature cortex

Olga Garaschuk[1,2], Jennifer Linn[2], Jens Eilers[2,3] and Arthur Konnerth[1,2]

[1] *Institut für Physiologie, Technische Universität München, 80802 München, Germany*

[2] *Physiologisches Institut, Universität des Saarlandes, 66421 Homburg, Germany*

[3] *Present address: Department of Neurobiology, Duke University Medical Center, Durham, North Carolina, 27710, USA*

Correspondence should be addressed to A.K. (konnerth@physiol.med.tu-muenchen.de)

Two-photon imaging of large neuronal networks in cortical slices of newborn rats revealed synchronized oscillations in intracellular Ca^{2+} concentration. These spontaneous Ca^{2+} waves usually started in the posterior cortex and propagated slowly (2.1 mm per second) toward its anterior end. Ca^{2+} waves were associated with field-potential changes and required activation of AMPA and NMDA receptors. Although $GABA_A$ receptors were not involved in wave initiation, the developmental transition of GABAergic transmission from depolarizing to hyperpolarizing (around postnatal day 7) stopped the oscillatory activity. Thus we identified a type of large-scale Ca^{2+} wave that may regulate long-distance wiring in the immature cortex.

Spontaneous correlated neuronal activity represents a hallmark of the developing central nervous system (see refs. 1–4 for review). The mechanisms underlying these spontaneous oscillations are highly distinct and include communication through gap junctions and Ca^{2+} release from intracellular Ca^{2+} stores in the cortex[5,6], activation of acetylcholine receptors in the retina[7] and the depolarizing action of $GABA_A$ receptors in the hippocampus[8,9]. The oscillations differ not only in the underlying mechanisms, but also in their specific patterns. For example, retinal waves are initiated at random locations and travel in different directions through a subset of retinal cells[7,10]. The same retinal cell can sequentially participate in different waves of activity that travel in various directions. By contrast, the hippocampal early network oscillations represent stereotypical activity patterns that involve the whole neuronal population and recur with regular frequency[9]. The region specificity of the spontaneous oscillatory activity patterns is believed to promote the establishment of region-specific connections[11].

So far, spontaneous oscillatory activity in the immature neocortex is detected only in individual cells[12,13], in cell pairs[14] or in rather small groups of 5–50 neurons, so-called 'neuronal domains'[5]. These spontaneous cortical activities are also very different mechanistically. They are mediated either by activation of metabotropic glutamate[13] or $GABA_A$[12] receptors or by passage of IP_3 through gap junctions[6]. The restricted amount of synchronous oscillatory activity in the neonatal cortex and the small size of spontaneously active neuronal domains seem to be consistent with the very low density of synaptic contacts, as demonstrated both morphologically[15,16] and functionally[17]. However, it remains unclear how such local types of neuronal activities can promote the establishment of long-range neuronal connections, which are typical for both excitatory and inhibitory neurons in the adult cortex[18] and are found in the developing visual cortex already at the time of eye opening, before extensive visual experience[19,20]. These long-range connections are thought to represent the morphological basis for 'binding' signals—oscillatory electrical activity underlying the reintegration or 'binding' of information acquired by different receptive fields into a single perceptual entity[21].

Here we identified a form of large-scale spontaneous oscillatory activity using two-photon imaging to simultaneously monitor intracellular calcium concentration ($[Ca^{2+}]_i$) in thousands of cortical neurons in newborn rat slices. In marked contrast to previously detected activities, these cortical early network oscillations involved the entire network of neurons, were highly correlated across the cortical slice and consisted of Ca^{2+} waves propagating along the longitudinal axis of the cortex, crossing anatomical boundaries between different cortical subregions.

Results

Our approach enabled real-time functional analyses of fairly large cortical networks in the immature rodent brain (**Fig. 1**). We prepared acute brain slices of the desired brain region (**Fig. 1a** and **c**) and then stained the cells with a fluorescent, membrane-permeable ion indicator dye[12,22]. For example, the Ca^{2+} indicator dye fura-2 AM routinely stained all neurons within the top 50–150 μm of the slices efficiently. When imaging this preparation with a two-photon laser scanning microscope[23,24], we could simultaneously monitor thousands of neurons in a thin 'optical' section within the slice[24]. The improved depth penetration and the high sensitivity of two-photon imaging[25,26] allowed us to record at a depth at which we would expect cells to be minimally, if at all, affected by the slicing procedure. Images were obtained at various magnifications (**Fig. 1c–e**). At high magnifications, individual neurons and their dendrites could be resolved (**Fig. 1e**) and functionally analyzed. Recordings with a good signal-to-noise ratio were obtained at relatively low excitation intensities. Under these conditions, no significant photobleaching or photodamage was observed; thus, it was possible to measure fluorescence continuously for long periods (up to eight hours).

We used two-photon imaging to investigate the cellular activities in brain slices from newborn rats. Surprisingly, instead

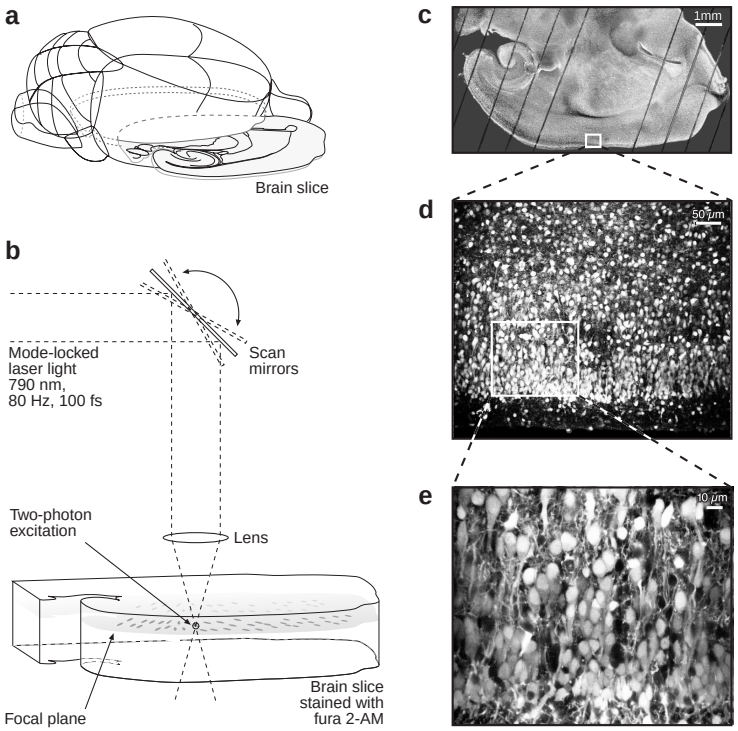

Fig. 1. Two-photon Ca^{2+} imaging in large neuronal assemblies. (**a**) Schematic drawing of the neonatal rat brain. Dotted lines delineate the region from which cortical slices were obtained. (**b**) Illustration of the experimental arrangement. Note that fluorescence, generated by two-photon excitation, is restricted to the focal plane. (**c**) Two-photon fluorescence image of a cortical slice from a 2-day-old rat taken at a low magnification (1.9× objective). Scale bar, 1 mm. In this and the following figures, nylon threads used to keep the brain slice in place appear as dark transverse lines. The cortical region delimited by the white box is shown at a higher magnification (20× objective; **d**). Scale bar, 50 µm. (**e**) At the highest magnification (60× objective), individual cells and their dendritic process are well resolved. Scale bar, 10 µm.

of small active domains[5], prolonged examination of slices from one- or two-day-old (P1–P2) rats (**Fig. 2a**) revealed prominent spontaneous, transient elevations in the intracellular Ca^{2+} concentration that occurred globally throughout the cortex (**Fig. 2b**). These Ca^{2+} transients recurred at very low rates (approximately once per 1–12 minutes; **Fig. 2e** and **f**) and were correlated throughout the entire cortical slice over distances of 8 millimeters or more. Each trace in Fig. 2b shows population responses from about 5000 neurons recorded at low magnification. These spontaneous network oscillations of intracellular Ca^{2+} levels were a robust phenomenon that persisted for many hours with little alteration, even after over seven hours of continuous fluorometric recordings (**Fig. 2d**). Individual waves occurred either as bursts of Ca^{2+} transients, mostly in the posterior (entorhinal) and the anterior (perirhinal/insular) region, or as single transients in the middle portion (temporal/perirhinal) of the cortex (**Fig. 2c**). In recordings from seven slices, the activity was analyzed in the different anatomical layers of the temporal/perirhinal cortex. We found that the activity was always present in all cortical layers, further indicating that the whole cortical network was involved in this large-scale spontaneous neuronal activity. Therefore, we termed this new form of spontaneous activity cortical early network oscillations (cENO).

In view of the weakly developed synaptic connectivity in the cortex of neonates[3,15–17,27], it is important to know how many neurons participate in the cENOs. Comparison of the population activity recorded in a region covering 38 neurons (**Fig. 3a–c**) to the activity registered in 2 individual neurons of this group (**Fig. 3d**) demonstrated a tight correlation of most signals. Asynchronous, small Ca^{2+} signals were sometimes detected in the individual neurons (**Fig. 3d**). These Ca^{2+} transients may be associated with action potentials firing out of phase. The cENO-associated Ca^{2+} transients were not restricted to the cell bodies but were always present in the main apical dendrite of each pyramidal neuron (**Fig. 3d**). Interestingly, cENO-associated Ca^{2+} transients were detected in almost all neurons (32 of 38) within the cortical region shown in Fig. 3b. In another experiment, more than 100 cells were analyzed (**Fig. 3e**). Again, most neurons of this group responded during almost every wave of the cENOs with a high degree of synchrony. Taken together, such analyses of 771 cells in 11 slices (groups of 30–200 cells) revealed that 87 ± 3% of the neurons examined participated in the cENOs.

The cENO-associated Ca^{2+} transients were closely correlated with changes in the field potential (**Fig. 3f**) recorded with extracellular electrodes. Similar cENO-associated changes in field potential were also observed in non-stained and non-imaged slices (**Fig. 3g**), indicating that neither the staining procedure nor the imaging-associated illumination significantly affected the oscillatory activity. Field potential transients had comparable amplitudes and durations in both cases (**Fig. 3h**). Notably, the amplitudes of the field potentials were very small both in stained (51 ± 4 µV, $n = 47$ events, 4 slices, P3–P5 rats) and in non-stained slices (63 ± 2 µV, $n = 304$ events, 5 slices, P4 rats), with a signal-to-noise ratio that was far inferior to that obtained by Ca^{2+} imaging.

When examined at higher temporal resolution by using line-scan recordings (sampling rate 160 Hz), each oscillatory event represented a spreading wave of activity (**Fig. 4**). A Ca^{2+} wave (**Fig. 4a**) was monitored at three points over a distance of 4.7 mm to yield posterior, intermediate and anterior time traces (**Fig. 4b**). At higher magnification (**Fig. 4c–e**), the propagation could be easily resolved at the level of individual neurons as a series of sequential responses. In the majority of cases (84 ± 7%, $n = 18$ slices), the waves of activity propagated from posterior to anterior within the slice (**Fig. 4a–f**). However, in 7 of 18 slices, we also observed waves traveling in the opposite direction (**Fig. 4e** and **f**). Propagation speeds measured on the level of single cells (2.0 ± 0.4 mm per s, $n = 8$ slices) and for long-range propagation (2.1 ± 0.5 mm per s, $n = 5$ slices; **Fig. 4g**) were similar. The speed of propagation in the opposite, anterior-to-posterior direction (1.6 ± 0.3 mm per s; $n = 4$ slices) was slightly, but not significantly ($p = 0.45$, Student's two-tailed t-test), smaller then the speed of propagation in the posterior-to-anterior direction. When the line-scan measurements were conducted in the vertical direction, across cortical layers ($n = 8$ slices, 16 locations in entorhinal, temporal and perirhinal cortices), the cENOs were detected in all layers almost simultaneously, with only small deviations along the vertical axis toward the cortical surface.

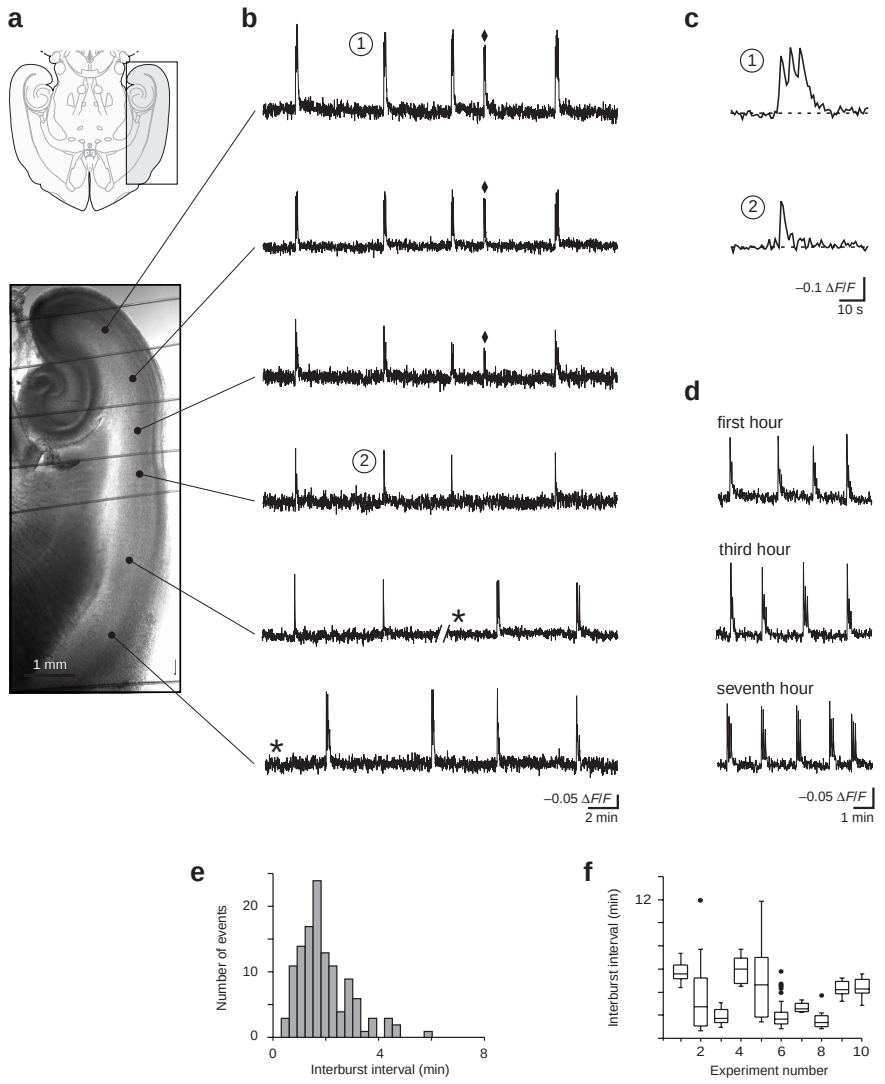

Fig. 2. Spontaneous oscillatory Ca^{2+} waves in the immature cortex. (**a**) The box in the schematic drawing of a horizontal section of the brain (top) delimits the cortical region shown in the photomicrograph (bottom). Slice preparation from a two-day-old rat. Black dots indicate the position of non-overlapping regions of interest (covering about 1 mm^2) from which the activity-dependent fluorescence was recorded (see **b**). Scale bar, 1 mm. (**b**) Fluorometric Ca^{2+} recordings from the sites indicated in (**a**). In this and in the following figures, fluorescence data are expressed as $-\Delta F/F$ (background-corrected decrease in fluorescence divided by the resting fluorescence). (**c**) Ca^{2+} transients labeled with '1' and '2' shown at a higher temporal resolution. To monitor activity in the whole preparation, the recording was made in two steps using overlapping frames. Asterisks mark traces obtained during the second recording step. Note that Ca^{2+} bursts marked with diamonds did not occur at all sites. (**c**) Ca^{2+} transients (corresponding to events marked in **b**) on an expanded time scale. Note different response patterns in different cortical areas. (**d**) Ca^{2+} oscillations in the entorhinal cortex of a one-day-old rat recorded continuously for seven hours. (**e**) Interval histogram (bin width, 18 s) of 122 intervals between the Ca^{2+} waves recorded in the experiment in (**d**). Interburst intervals are measured between the starts of two consecutive Ca^{2+} bursts. (**f**) Box plot of interburst intervals from ten experiments using one- to two-day-old rats. Data are expressed as median (line), interquartile (box), outliers (filled circles) and the farthest points that are not outliers (extended lines). Experiments illustrated in (**a–c**) and (**d**, **e**) refer to slice numbers 4 and 6, respectively.

We next examined the mechanisms underlying the initiation of cENOs. In contrast to gap junction-mediated activity in cortical domains, the cENOs were completely and reversibly blocked by tetrodotoxin (TTX, 250 or 500 nM; $n = 7$ slices; **Fig. 5a** and **c**). Furthermore, the frequency of the cENOs was reduced by lowering the temperature from 32°C to 20°C (78 ± 19% of control, $n = 5$; $p = 0.22$, Student's two-tailed t-test; **Fig. 5b** and **d**), and not enhanced, as found for the activity in cortical domains[28]. In addition, the number of Ca^{2+} transients within the cENO-associated Ca^{2+} burst decreased at 20°C to 59 ± 9% of the control value (**Fig. 5e**). The cENOs were also completely and reversibly blocked by a mixture of ionotropic GABA- and glutamate receptor antagonists (10 μM CNQX + 50 μM D,L-APV + 20 μM bicuculline, $n = 5$) and thus they seem to require active chemical synapses. When the effects of these antagonists were studied separately, we found that CNQX completely and reversibly blocked cENOs even at concentrations as low as 2 μM ($n = 6$, **Fig. 6b** and **e**), whereas even 20 μM bicuculline failed to block cENOs ($n = 9$, **Fig. 6d** and **e**). The cENOs were also completely and reversibly blocked by 50 μM APV ($n = 5$). The effects of blockers were independent of the age of the rat (one to five days) from which the slices were obtained. Both CNQX and APV blocked cENOs in all cortical regions throughout the slice, suggesting that the activation of ionotropic glutamate receptors is essential for initiation of cENOs. The experiments also demonstrated some distinctive functional properties of cENOs (**Fig. 6**). Besides the much higher rates of repetition of hippocampal early oscillations as compared with those detected in cortex, antagonists of AMPA and of $GABA_A$ receptor channels had opposite, reciprocal effects in these two regions (**Fig. 6b** and **d**) in all seven slices tested. Even at P1, the cENOs critically depended on activation of AMPA receptors and made no use of the depolarizing GABAergic transmission (**Fig. 6b** and **d**).

An additional distinctive feature of cENOs was their rapid, region-specific developmental changes in the frequency of oscillation during the first postnatal days. The network oscillations emerged after birth as a rather coherent activity in the majority of neurons of the entire cortex (92 ± 3% coherency, $n = 347$ waves, 11 slices, 8 rats; **Fig. 2b**). The median interval between individual waves was around four minutes in all cortical subregions (**Figs. 2f** and **7b**). During the following days of development, the frequencies of activity recorded in the posterior (entorhinal cortex)

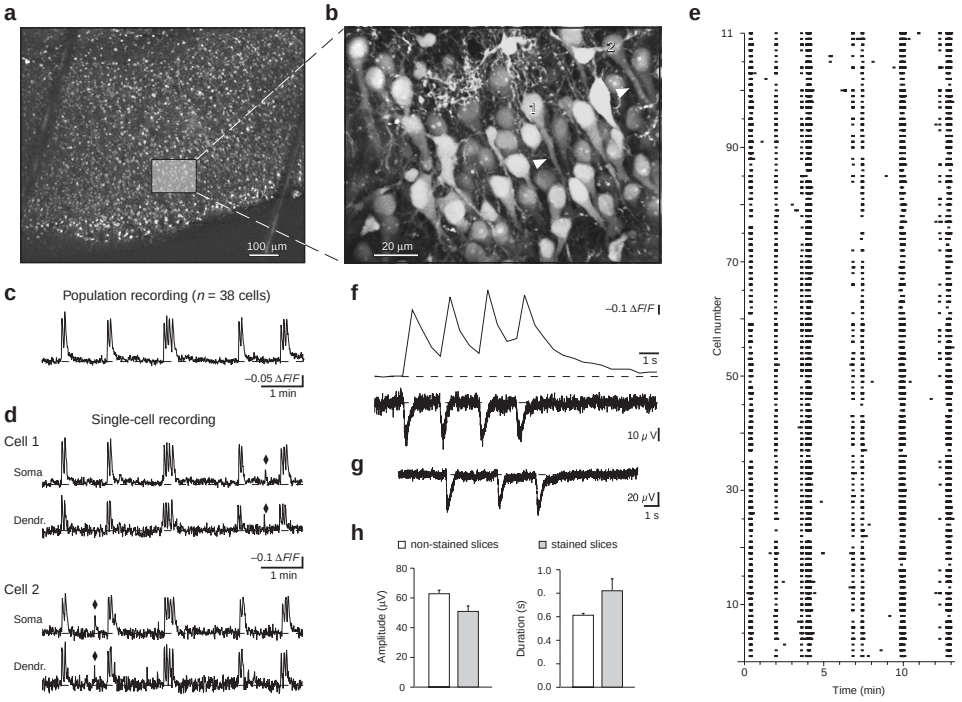

Fig. 3. Cortical early network oscillations involve the majority of cortical neurons. (**a**) Two-photon fluorescence image from the temporal cortex of a 3-day-old rat acquired 60 µm below the surface of the slice with a 10x objective. The region delimited by the shaded box is shown at a higher magnification in (**b**). Scale bar, 100 µm. (**b**) High-resolution fluorescence image of layer II/III showing individual cells and their neurites. The image represents a *x*–*y* projection of the stack of images taken from 56–64 µm below the surface of the slice (*z*-step, 0.5 µm). Ca^{2+} signals from cell '1' and '2' are shown in (**d**). Arrowheads point toward the dendrites of these two cells. Scale bar, 20 µm. (**c**) Population Ca^{2+} recordings obtained by averaging cENO-associated fluorescence transients obtained from 38 individual neurons that can be unambiguously distinguished in (**b**). (**d**) Ca^{2+} recordings from the somata and the dendrites of two cortical cells (corresponding to the sites marked in **b**). Note that cENO-associated Ca^{2+} bursts detected in single cells are synchronous with those observed in the population recording (**c**). The diamonds indicate asynchronous Ca^{2+} transients. (**e**) Ca^{2+} transients recorded simultaneously in 110 cells. Data were reduced to a binary form by setting a threshold of four times the root mean square value of the resting fluorescence of recordings from individual cells. (**f**) Population Ca^{2+} response (upper trace) and field potential changes (lower trace) recorded simultaneously in the same region of the temporal cortex of a five-day-old rat. (**g**) Field potential recordings in the temporal cortex of a four-day-old rat obtained in a non-stained slice. (**h**) Bar graphs illustrating the mean amplitudes (left) and durations (right) of cENO-associated changes in field potential measured in non-stained (n = 5, 304 events) and fura-2 AM-loaded (n = 4, 47 events) slices.

or in the more anterior cortical regions diverged rapidly (**Fig. 7a**). Whereas the rate remained almost constant until P4 and then steeply increased at P5–P6 in the entorhinal cortex, it continuously dropped in the temporal/perirhinal/insular cortex, reaching values of 1 wave per 20–50 minutes at P4 (**Fig. 7a** and **b**). Note that the majority (74 ± 13%, n = 38 waves, 7 slices) of these Ca^{2+} waves were correlated with one of the more frequently occurring waves in the posterior cortex (**Fig. 7a**), and only 26% were more localized and restricted to the perirhinal/insular cortex. Furthermore, the Ca^{2+} waves maintained their region-specific patterns at least until P5. Thus the oscillatory activity in the entorhinal cortex was characterized by bursts of Ca^{2+} transients (on average, 2.5 ± 0.3 Ca^{2+} transients per burst; n = 26 slices), whereas in all other areas it consisted of a mixture of single and paired Ca^{2+} transients. In all areas studied, we occasionally observed large bursts comprising up to 4–6 Ca^{2+} transients. For better quantitation, the baseline-subtracted area under the measured fluorescence trace was taken as an integral measure of the strength of cENOs[9]. In all cortical subregions, the area progressively decreased with development (**Fig. 7c**) and, finally, no cENOs were detected in the cortex after P6. This decrease in the overall activity, however, showed region specificity. In the entorhinal cortex, the developmental increase in frequency was paralleled by a significant decrease in the amplitude, whereas the amplitude of the cENO-associated Ca^{2+} transients in the anterior cortex remained constant but their frequency decreased considerably (**Fig. 7a** and **b**; note different scaling of the traces in **a**). No cENOs were observed in the anterior cortex beyond P5, even during long periods (two to three hours) of continuous recording.

A final set of results provided evidence that the developmental disappearance of cENOs may be determined by the switch from GABAergic excitation to inhibition. Consistent with this assumption, we found that the mean amplitude of GABA-mediated Ca^{2+} transients gradually decreased during postnatal development (**Fig. 8**). By using the ratio of GABA- against KCl-evoked Ca^{2+} transients, we found that the amplitudes of the responding neurons reached a minimal value around P5 (**Fig. 8e**). From birth until P5/P6, during the time of the most intensive cENO activity, more than 90% of all examined cortical neurons produced GABA-mediated Ca^{2+} transients (**Fig. 8a**, **b** and **f**). Around P7/P8, the time at which cENOs are no longer detected, however, the proportion of the responding neurons dropped to 41% (**Fig. 8f**). Furthermore, bicuculline, which was ineffective in blocking the initiation of cENOs (**Fig. 6d** and **e**) induced oscillatory cENO-like Ca^{2+} waves in slices from rats 7 or more days old (n = 4; **Fig. 7d**). Taken together, these findings clearly indicate that, whereas GABAergic excitation was unnecessary for initiation of cENOs early after birth, overall GABAergic inhibition beyond P7/P8 was sufficiently strong to suppress cENOs.

Discussion

Two-photon Ca^{2+} imaging revealed a previously undescribed type of spontaneous activity in the developing cortex. The TTX sensitivity of these cENOs and their dependence on activation of ionotropic glutamate receptors suggest that they require synap-

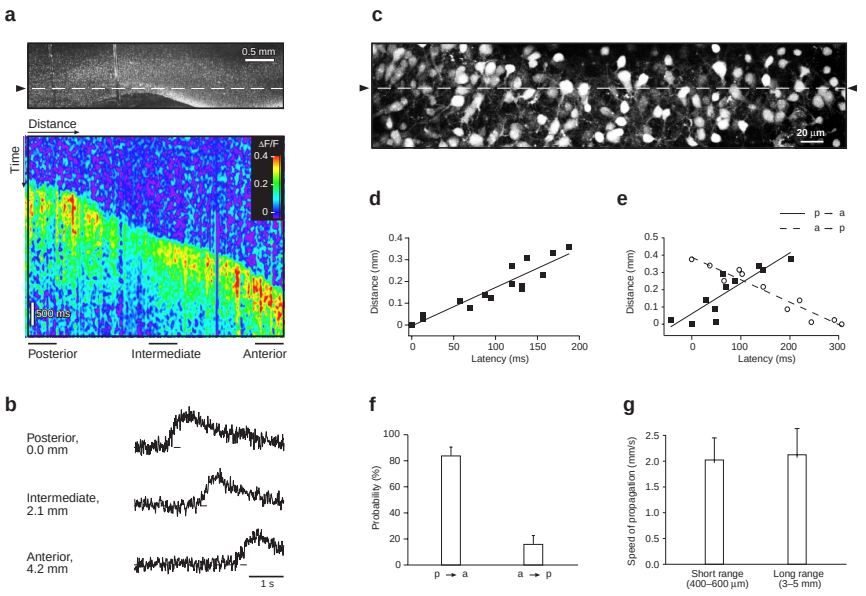

Fig. 4. Transcortical propagation of cENO-associated Ca^{2+} waves. (**a**) Top, fluorescence image of the temporal cortex of a one-day-old rat. Here and in (**c**), the dashed line indicates the site of line-scan recordings. Bottom, line-scan recording of a Ca^{2+} wave. (**b**) Normalized fluorescence signals from three cortical regions as indicated in (**a**, bottom). The distance relative to the posterior region is indicated next to each trace. (**c**) Fluorescence image of cells of layer II/III in the posterior part of the temporal cortex (60 µm below the slice surface) from a 3-day-old rat. (**d**) Latency of the onset of a Ca^{2+} wave in cells crossed by the scan line in panel (**c**) plotted against their distance to the leftmost cell in (**c**). The Ca^{2+} wave propagated from the posterior to the anterior cortex. The solid line represents a linear least-square fit with a slope of 1.8 mm per s. (**e**) Same analysis as in (**d**) in an experiment in which Ca^{2+} waves propagated in both directions, posterior-to-anterior (filled symbols) and anterior-to-posterior (open symbols). The solid and dashed lines represent linear least-square fits to the respective sets of data with slopes of 1.7 mm per s and –1.3 mm per s. (**f**) Plot of the probability of Ca^{2+} oscillations propagating in either direction (n = 18 slices). (**g**) Comparison of the speed of propagation of the Ca^{2+} waves between single cells (short range, n = 8 slices) and large cortical regions (long range, n = 5 slices).

tic transmission. This contrasts with other previously described forms of spontaneous correlated activity in the immature cortex[5,14]. It remains to be investigated whether the action of glutamate during cENOs is mediated solely through conventional synapses, or whether it also involves spillover of transmitter from conventional synapses to extrasynaptic receptors[29] and/or non-synaptic release of transmitter, as is suggested for taurine[30]. The importance of AMPA receptors for the initiation of cENOs was unexpected in view of GABA's widespread depolarizing action in the immature cortex[12,22] and its importance in generation of hippocampal ENOs[9,31]. However, the cortical early network oscillations, unlike the hippocampal ones, persisted in bicuculline. Even at P1, the cENOs were extremely sensitive to low concentrations of CNQX (2 µM), which only partially blocked AMPA receptors[32]. This suggests that in the developing cortex, synapses with functional AMPA receptors have a much more pronounced impact than in the hippocampus at the same age, where 80% of all glutamatergic synapses are 'silent'[33]. Thus, the maturation of excitatory glutamatergic transmission in the cortex seems to occur earlier than in the hippocampus, in line with findings that only 34% of all thalamocortical synapses are silent at P2 (ref. 34).

A characteristic feature of cENOs was their propagation along the longitudinal axis of the cortex. The average speed of propagation of cENO-associated Ca^{2+} waves was 2 mm per second, different from the speeds of propagation found within cortical domains (100 µm per second; ref. 28), in the retina (200–400 µm per second; ref. 35) or in the hippocampal formation (8 mm per second; ref. 36). Although the usual cortical 'pacemaker' seemed to be located in the entorhinal cortex, cENOs were also sometimes found to emerge from anterior cortical regions. This suggests that more than one region is a potential pacemaker of cENOs. Remarkably, the speed of propagation of cENOs is most similar to the mean velocity found for the spread of non-synaptic epileptiform activity in the adult hippocampus (1.7 mm per

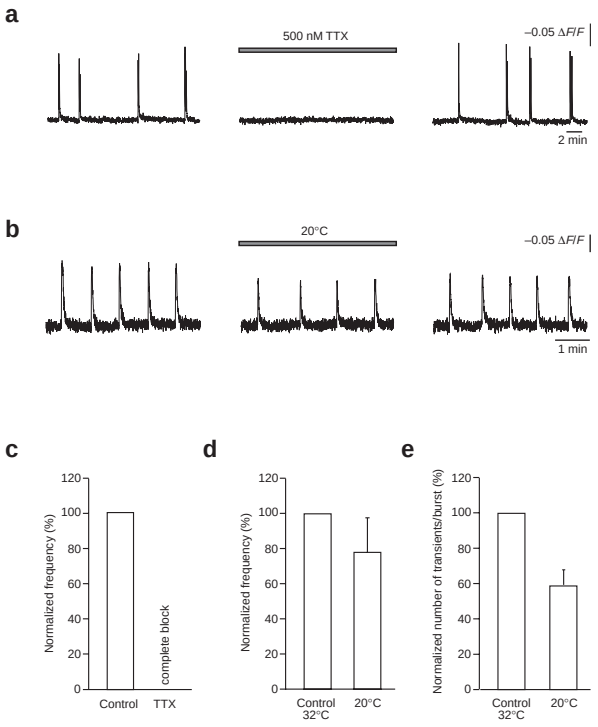

Fig. 5. The cENOs are preserved at room temperature and blocked by tetrodotoxin. (**a**) cENOs recorded in the temporal cortex of a 1-day-old rat in control (left), in the presence of 500 nM TTX (middle) and after washout of TTX (right). (**b**) cENOs recorded in the temporal cortex of a 2-day-old rat in control conditions (left), at 20°C (middle) and after return to 32°C (right). (**c**–**e**) Plots of the relative (normalized to control) frequency of Ca^{2+} oscillations (**c**, **d**) and of the relative number of Ca^{2+} transients within the cENO-associated Ca^{2+} burst (**e**) during the application of 250 or 500 nM TTX (**c**) and during the change in temperature (**d**, **e**). Each bar shows an average of seven experiments.

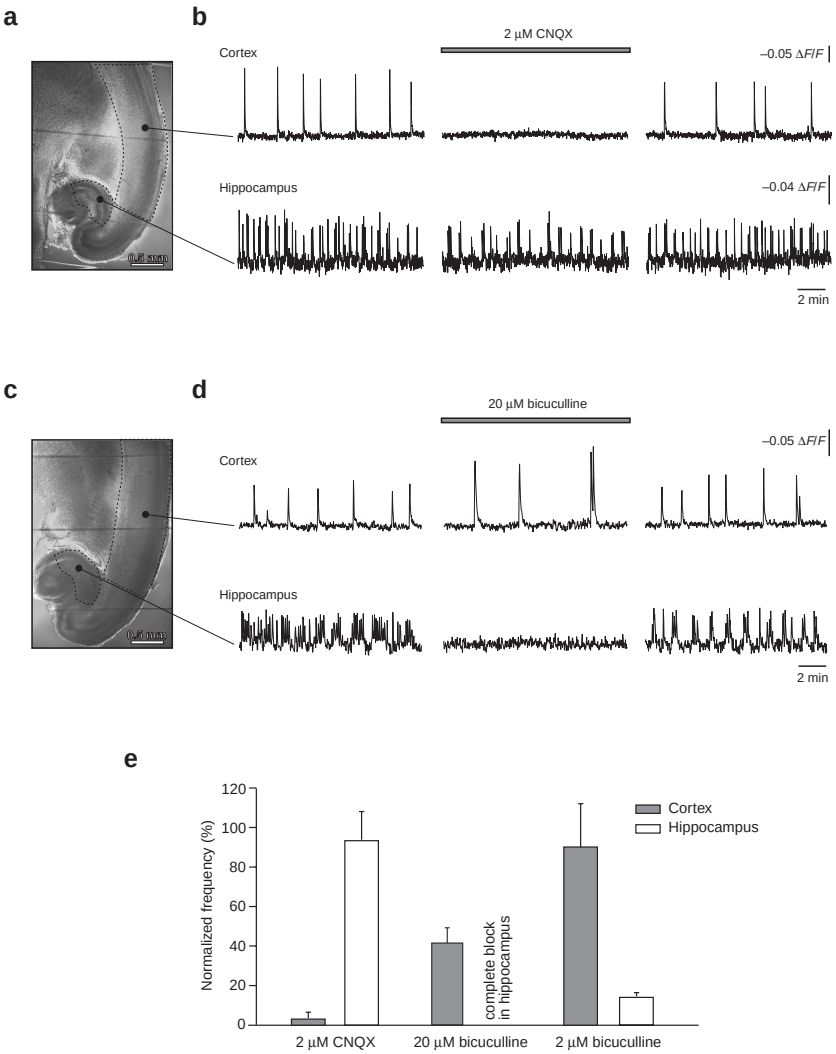

Fig. 6. Striking differences between cortical and hippocampal early network oscillations. (**a**) Microphotograph of a horizontal brain slice from a 1-day-old rat taken at low magnification (4× objective). Regions of interest from which the recordings shown in (**b**) were obtained are indicated. (**b**) Simultaneous fluorometric recordings from cortical (upper panel) and hippocampal (lower panel) regions in a control (left), in the presence of 2 μM 6-cyano-7-nitroquinoxaline-2,3-dione (CNQX, middle) and after washout of CNQX (right). (**c, d**) Experiment similar to the one shown in (**a**, **b**) illustrating the effect of 20 μM bicuculline. The slice was obtained from a one-day-old rat. Note that whereas the reduction in frequency of cortical ENOs was robust (see panel **e**), increased amplitude was observed only in five of nine slices. (**e**) Plot of the mean relative (normalized to control) frequency of Ca^{2+} oscillations in the cortex (filled bars) and in the hippocampus (open bars) in the presence of 2 μM CNQX (n = 6), 20 μM bicuculline (n = 9) and 2 μM bicuculline (n = 6).

second), which involves the sequential recruitment of inactive neurons through a wave of extracellular K^+ released by active neurons[37].

What might be the function of cENOs? In the immature central nervous system, transient elevations of the intracellular Ca^{2+} concentration are important in many aspects of growth and differentiation. These include proliferation[38], gene expression[39,40], neuronal migration[41], motility of axonal and dendritic growth cones[42], clustering of the postsynaptic receptor-channels[43] and activity-dependent maturation of glutamatergic synapses[33]. Many of these Ca^{2+}-dependent processes require repeated, cyclic changes of the intracellular Ca^{2+} level: in the developing spinal cord[44], for example, the speed of growth cone migration is controlled by the frequency of spontaneously occurring Ca^{2+} transients. Therefore, growth cones experiencing a high frequency of Ca^{2+} transients (10–12 per h) migrate slowly or retract, whereas growth cones experiencing a low frequency of Ca^{2+} transients (0–0.4 per h) migrate rapidly. As the cENOs are comparable in frequency and involve large populations of neurons, they represent a prime candidate to promote neuronal development and to 'synchronize' development over large cortical regions.

In conclusion, our results indicate that the spontaneous patterned activity in the developing cortex is far more complex than has been previously anticipated. It seems to consist of large-scale cENOs acting in concert with more localized, mechanistically distinct oscillations[5,14]. Although all types of synchronous activity may sculpt neuronal circuits by reinforcing connections among coactive cells[3], their specific assignments may differ. Because of the radial organization and distinct borders of the local domains, correlated activity within these structures would promote the columnar organization of the cortex[5], whereas cENOs would be particularly important for the establishment of long-range neuronal connections. Thus, during the earliest postnatal stages, the intrinsic cENOs might serve as a pacemaker that determines a coherent and coordinated development of the weakly interconnected cortical subregions.

Methods

All experimental procedures were approved by local government authorities. Horizontal cortical slices (400–500 μm) were prepared from 116 Wistar rats aged from P0 (the day of birth) to P12, as previously described[45,46]. The extracellular solution was continuously bubbled with 95% O_2 and 5% CO_2 at 32°C and contained 125 mM NaCl, 4.5 mM KCl, 2 mM $CaCl_2$, 1 mM $MgCl_2$, 1.25 mM NaH_2PO_4, 26 mM $NaHCO_3$ and 20 mM glucose at pH 7.4. For fluorometric Ca^{2+} measurements, slices were loaded with the membrane-permeable form of fura-2 (fura-2 AM, Molecular Probes, Eugene, Oregon or fura-PE3 AM, TefLabs, Austin, Texas) using standard procedures[9].

Fluorometric recordings were made using a custom-built two-photon laser-scanning microscope[23] based on a Ti:sapphire laser system ('Tsunami' and 'Millennia', both from Spectra-Physics, Mountain View, California) that provided mode-locked laser light (pulse width <100 fs; repetition rate, 80 MHz, center wavelength, 790 nm) and a laser-scanning system (MRC 1024, Bio-Rad, Herts, UK) attached to an upright microscope (BX 50 WI, Olympus, Tokyo, Japan). Either water-immersion objectives (10×, 0.3 NA; 40×, 0.8 NA; 60×, 0.9 NA; all from Olympus) or dry objectives (1.9×, 0.14 NA, Olympus; 5×, 0.25 NA, Zeiss, Oberkochen, Germany) were used. For recordings with dry objectives, the recording chamber was sealed with a 0.13 mm-thick cover glass (Fisher Scientific, Pittsburgh, Pennsylvania) to prevent image distortion due to fluctuations in the bath solution level. Image analyses were

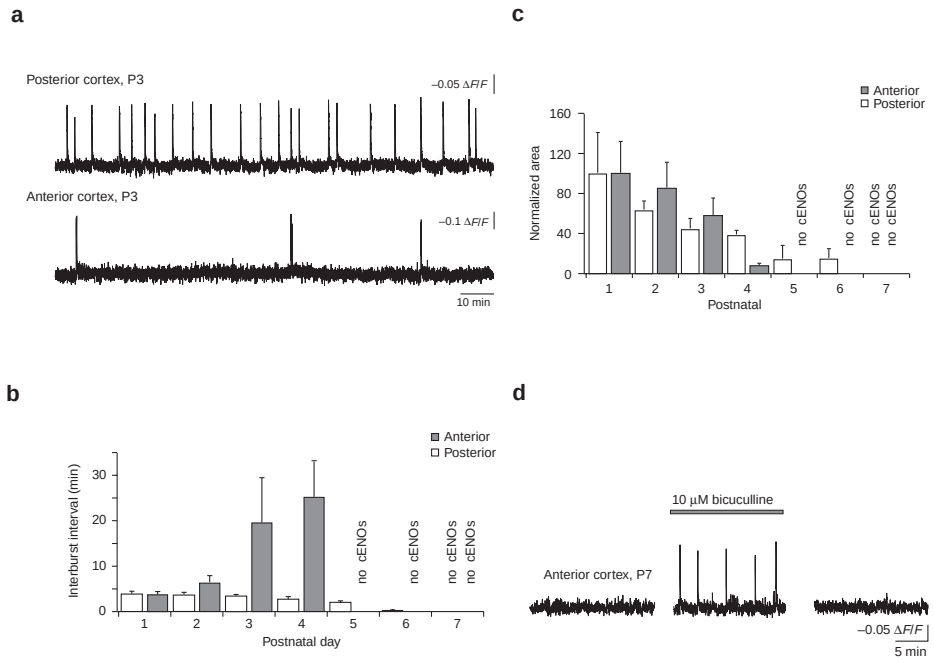

Fig. 7. Developmental confinement of early network oscillations to the first few days after birth. (**a**) Two-hour-long continuous fluorometric recordings from the entorhinal (posterior) and the perirhinal/insular (anterior) cortices in a slice from a three-day-old rat. (**b**) Averaged data showing the interburst intervals in the posterior and the anterior cortical regions plotted against postnatal age. Data are expressed as the mean value of the median interburst interval from 4–12 experiments per data point. (**c**) Averaged data showing the mean baseline-subtracted areas under the fluorescence traces (see Methods) as a function of the postnatal age. The area measurements were normalized with respect to the mean value obtained at P1. (**d**) Fluorometric recordings from the anterior cortex at P7 in control (left), in the presence of 10 μM bicuculline (middle) and after washout of bicuculline (right).

performed off-line with routines written in Labview and Igor Pro software (National Instruments, Austin, Texas and Wavemetrics, Eugene, Oregon, respectively).

Extracellular field potentials were low-pass filtered at 1 kHz, recorded with a custom-made DC amplifier and digitized at 5 kHz with an A/D converter (ITC 16, Instrutech, Port Washington, New York) controlled by Pulse software (HEKA, Lambrecht, Germany). The recording microelectrodes (resistances of 0.9–1.2 MΩ) were filled with 3 M NaCl and positioned in layer II/III of the cortex. GABA- and K^+-containing solutions were pressure-applied from fine pipets (resistances of 6–12 MΩ when filled with extracellular solution) using a Picospritzer II (General Valve, Fairfield, New Jersey). To obtain saline containing 80 mM K^+, 80 mM NaCl was substituted for KCl in the standard extracellular solution. The tips of both drug application pipets were placed near (~5 μm) the target neuron. Brief (500 ms) applications of the drugs usually evoked a Ca^{2+}-response in this neuron and in adjacent secondary neurons within a radius of ~5 μm. We used only primary target neurons for the amplitude analysis, whereas we also included the immediately adjacent secondary neurons in the calculation of the total number of responding cells. We determined the baseline-subtracted areas under fluorescence

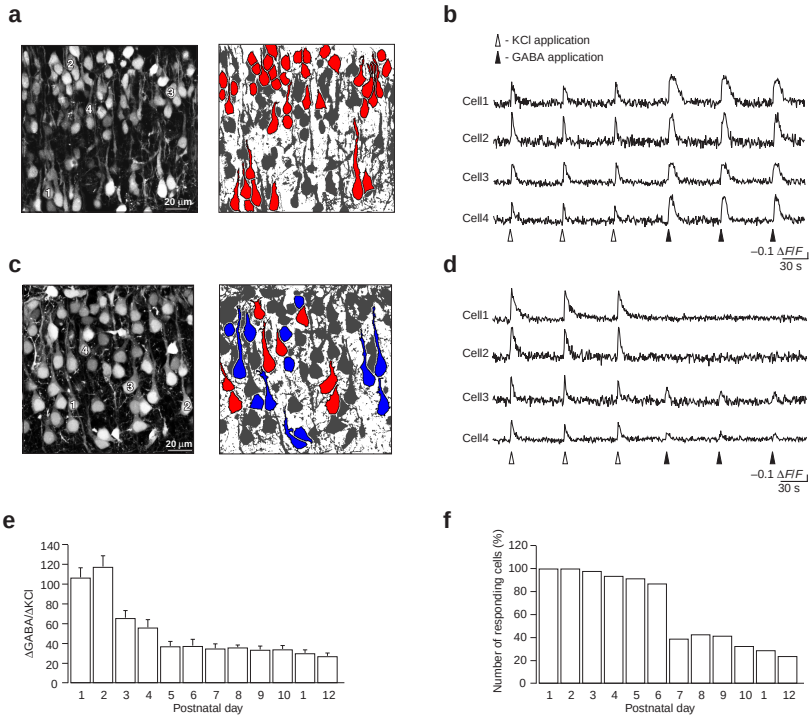

Fig. 8. GABA-activated Ca^{2+} transients in the immature cortex. (**a**) Left, high-resolution fluorescence image of cells in layer II/III of the temporal cortex of a 1-day-old rat taken with a 60× objective. Right, the same image transformed into black and white mode by using a threshold function. Here and in (**c**), cells to which GABA was pressure-applied are color coded. Cells that responded to GABA application with a Ca^{2+} transient are shown in red. (**b**) Fluorometric recordings from neurons marked with corresponding numbers in (**a**). Ca^{2+} transients were activated either by 500 ms applications of 80 mM K^+ (open triangles) or by 500 ms applications of 100 μM GABA (filled triangles). (**c**, **d**) Analyses similar to those shown in (**a**, **b**) in the temporal cortex of an eight-day-old rat. Cells that did not show Ca^{2+} elevations in response to GABA application (for example, cells 1 and 2 in **d**) are shown in blue. (**e**) The ratio of the amplitudes of GABA- versus K^+-evoked Ca^{2+} transients plotted against postnatal age. Analyses were conducted on 10–15 cells per age. Only the primary target cells (see Methods) were chosen for these analyses. (**f**) Percentage of cells showing GABA-activated Ca^{2+} transients plotted against postnatal age. The plot summarizes experiments conducted in 47–64 cells per data point.

traces as an integral strength parameter of cENOs that takes into account both the frequency and the amplitude of the oscillations for a defined series of oscillatory events[9]. Data are given as mean ± standard error of mean (s.e.).

Acknowledgements

We thank E. Brown for advice and help in developing the two-photon imaging set-up and E. Hanse and M. Noll-Hussong for participating in the preliminary experiments. We also thank A. Selyanko for comments on the manuscript and R. Trautmann, H. Krempel, E. Eilers and D. Hof for technical assistance. The work was supported by the HFSP and the Deutsche Forschungsgemeinschaft (SFB 391).

RECEIVED 4 FEBRUARY; ACCEPTED 9 MARCH 2000

1. Spitzer, N. C. Spontaneous Ca^{2+} spikes and waves in embryonic neurons: signaling systems for differentiation. *Trends Neurosci.* **17**, 115–118 (1994).
2. Constantine-Paton, M. & Cline, H. T. LTP and activity-dependent synaptogenesis: the more alike they are, the more different they become. *Curr. Opin. Neurobiol.* **8**, 139–148 (1998).
3. Katz, L. C. & Shatz, C. J. Synaptic activity and the construction of cortical circuits. *Science* **274**, 1133–1138 (1996).
4. Hanse, E., Durand, G. M., Garaschuk, O. & Konnerth, A. Activity-dependent wiring of the developing hippocampal neuronal circuit. *Sem. Cell Dev. Biol.* **8**, 35–42 (1997).
5. Yuste, R., Peinado, A. & Katz, L. C. Neuronal domains in developing neocortex. *Science* **257**, 665–669 (1992).
6. Kandler, K. & Katz, L. C. Coordination of neuronal activity in developing visual cortex by gap junction-mediated biochemical communication. *J. Neurosci.* **18**, 1419–1427 (1998).
7. Feller, M. B., Wellis, D. P., Stellwagen, D., Werblin, F. S. & Shatz, C. J. Requirement for cholinergic synaptic transmission in the propagation of spontaneous retinal waves. *Science* **272**, 1182–1187 (1996).
8. Leinekugel, X., Medina, I., Khalilov, I., Ben-Ari, Y. & Khazipov, R. Ca^{2+} oscillations mediated by the synergistic excitatory action of $GABA_A$ and NMDA receptors in the neonatal hippocampus. *Neuron* **18**, 243–255 (1997).
9. Garaschuk, O., Hanse, E. & Konnerth, A. Developmental profile and synaptic origin of early network oscillations in the CA1 region of rat neonatal hippocampus. *J. Physiol. (Lond.)* **507**, 219–236 (1998).
10. Wong, R. O., Chernjavsky, A., Smith, S. J. & Shatz, C. J. Early functional neural networks in the developing retina. *Nature* **374**, 716–718 (1995).
11. Penn, A. A., Riquelme, P. A., Feller, M. B. & Shatz, C. J. Competition in retinogeniculate patterning driven by spontaneous activity. *Science* **279**, 2108–2112 (1998).
12. Owens, D. F., Boyce, L. H., Davis, M. B. & Kriegstein, A. R. Excitatory GABA responses in embryonic and neonatal cortical slices demonstrated by gramicidin perforated-patch recordings and calcium imaging. *J. Neurosci.* **16**, 6414–6423 (1996).
13. Flint, A. C., Dammerman, R. S. & Kriegstein, A. R. Endogenous activation of metabotropic glutamate receptors in neocortical development causes neuronal calcium oscillations. *Proc. Natl. Acad. Sci. USA* **96**, 12144–12149 (1999).
14. Schwartz, T. H. *et al.* Network of coactive neurons in developing layer 1. *Neuron* **20**, 541–552 (1998).
15. Blue, M. E. & Parnavelas, J. G. The formation and maturation of synapses in the visual cortex of the rat. II. Quantitative analysis. *J. Neurocytol.* **12**, 697–712 (1983).
16. Juraska, J. M. & Fifkova, E. An electron microscope study of the early postnatal development of the visual cortex of the hooded rat. *J. Comp. Neurol.* **183**, 257–267 (1979).
17. Dalva, M. B. & Katz, L. C. Rearrangements of synaptic connections in visual cortex revealed by laser photostimulation. *Science* **265**, 255–258 (1994).
18. Braitenberg, V. & Schüz, A. *Anatomy of the Cortex* 141–146 (Springer, New York, 1991).
19. Galuske, R. A. & Singer, W. The origin and topography of long-range intrinsic projections in cat visual cortex: a developmental study. *Cereb. Cortex* **6**, 417–430 (1996).
20. Weliky, M. & Katz, L. C. Functional mapping of horizontal connections in developing ferret visual cortex: experiments and modeling. *J. Neurosci.* **14**, 7291–7305 (1994).
21. Singer, W. & Gray, C. M. Visual feature integration and the temporal correlation hypothesis. *Annu. Rev. Neurosci.* **18**, 555–586 (1995).
22. Yuste, R. & Katz, L. C. Control of postsynaptic Ca^{2+} influx in developing neocortex by excitatory and inhibitory neurotransmitters. *Neuron* **6**, 333–344 (1991).
23. Denk, W., Strickler, J. H. & Webb, W. W. Two-photon laser scanning fluorescence microscopy. *Science* **248**, 73–76 (1990).
24. Williams, R. M., Piston, D. W. & Webb, W. W. Two-photon molecular excitation provides intrinsic 3-dimensional resolution for laser-based microscopy and microphotochemistry. *FASEB J.* **8**, 804–813 (1994).
25. Yuste, R. & Denk, W. Dendritic spines as basic functional units of neuronal integration. *Nature* **375**, 682–684 (1995).
26. Svoboda, K., Denk, W., Kleinfeld, D. & Tank, D. W. *In vivo* dendritic calcium dynamics in neocortical pyramidal neurons. *Nature* **385**, 161–165 (1997).
27. Blue, M. E. & Parnavelas, J. G. The formation and maturation of synapses in the visual cortex of the rat. I. Qualitative analysis. *J. Neurocytol.* **12**, 599–616 (1983).
28. Yuste, R., Nelson, D. A., Rubin, W. W. & Katz, L. C. Neuronal domains in developing neocortex: mechanisms of coactivation. *Neuron* **14**, 7–17 (1995).
29. Kullmann, D. M., Erdemli, G. & Asztely, F. Long-term potentiation of AMPAR- and NMDAR-mediated signals: evidence for presynaptic expression and extrasynaptic glutamate spill-over. *Neuron* **17**, 1–20 (1996).
30. Flint, A. C., Liu, X. & Kriegstein, A. R. Nonsynaptic glycine receptor activation during early neocortical development. *Neuron* **20**, 43–53 (1998).
31. Ben-Ari, Y., Cherubini, E., Corradetti, R. & Gaiarsa, J. L. Giant synaptic potentials in immature rat CA3 hippocampal neurones. *J. Physiol. (Lond.)* **416**, 303–325 (1989).
32. Blake, J. F., Yates, R. G., Brown, M. W. & Collingridge, G. L. 6-Cyano-7-nitroquinoxaline-2,3-dione as an excitatory amino acid antagonist in area CA1 of rat hippocampus. *Br. J. Pharmacol.* **97**, 71–76 (1989).
33. Durand, G. M., Kovalchuk, Y. & Konnerth, A. Long-term potentiation and functional synapse induction in developing hippocampus. *Nature* **381**, 71–75 (1996).
34. Isaac, J. T. R., Crair, M. C., Nicoll, R. A. & Malenka, R. C. Silent synapses during development of thalamocortical inputs. *Neuron* **18**, 269–280 (1997).
35. Feller, M. B., Butts, D. A., Aaron, H. L., Rokhsar, D. S. & Shatz, C. J. Dynamic processes shape spatiotemporal properties of retinal waves. *Neuron* **19**, 293–306 (1997).
36. Leinekugel, X., Khalilov, I., Ben-Ari, Y. & Khazipov, R. Giant depolarizing potentials: the septal pole of the hippocampus paces the activity of the developing intact septohippocampal complex in vitro. *J. Neurosci.* **18**, 6349–6357 (1998).
37. Konnerth, A., Heinemann, U. & Yaari, Y. Slow transmission of neural activity in hippocampal area CA1 in absence of active chemical synapses. *Nature* **307**, 69–71 (1984).
38. LoTurco, J. J., Owens, D. F., Heath, M. J. S., Davis, M. B. E. & Kriegstein, A. R. GABA and glutamate depolarize cortical progenitor cells and inhibit DNA synthesis. *Neuron* **15**, 1287–1298 (1995).
39. Ghosh, A. & Greenberg, M. E. Calcium signaling in neurons: molecular mechanisms and cellular consequences. *Science* **268**, 239–247 (1995).
40. Gu, X. & Spitzer, N. C. Breaking the code: regulation of neuronal differentiation by spontaneous calcium transients. *Dev. Neurosci.* **19**, 33–41 (1997).
41. Komuro, H. & Rakic, P. Intracellular Ca^{2+} fluctuations modulate the rate of neuronal migration. *Neuron* **17**, 275–285 (1996).
42. Kater, S. B., Mattson, M. P., Cohan, C. & Connor, J. Calcium regulation of the neuronal growth cone. *Trends Neurosci.* **11**, 315–321 (1988).
43. Kirsch, J. & Betz, H. Glycine-receptor activation is required for receptor clustering in spinal neurons. *Nature* **392**, 717–720 (1998).
44. Gomez, T. M. & Spitzer, N. C. *In vivo* regulation of axon extension and pathfinding by growth-cone calcium transients. *Nature* **397**, 350–355 (1999).
45. Edwards, F., Konnerth, A., Sakmann, B. & Takahashi, T. A thin slice preparation for patch clamp recordings from neurones of the mammalian central nervous system. *Pflügers Arch.* **414**, 600–612 (1989).
46. Konnerth, A. Patch-clamping in slices of mammalian CNS. *Trends Neurosci.* **13**, 321–323 (1990).